PNAS RESEARCH ARTICLE | MEDICAL SCIENCES

Noncanonical PDK4 action alters mitochondrial dynamics to affect the cellular respiratory status

Themis Thoudam[a,1], Dipanjan Chanda[b,c,1], Ibotombi Singh Sinam[d,e], Byung-Gyu Kim[f], Mi-Jin Kim[a], Chang Joo Oh[a], Jung Yi Lee[b], Min-Ji Kim[g], Soo Yeun Park[h], Shin Yup Lee[g], Min-Kyo Jung[i], Ji Young Mun[i], Robert A. Harris[j], Naotada Ishihara[k,l], Jae-Han Jeon[g,2], and In-Kyu Lee[a,m,2]

Edited by Jodi Nunnari, University of California, Davis, Davis, CA; received November 4, 2021; accepted May 6, 2022

Dynamic regulation of mitochondrial morphology provides cells with the flexibility required to adapt and respond to electron transport chain (ETC) toxins and mitochondrial DNA-linked disease mutations, yet the mechanisms underpinning the regulation of mitochondrial dynamics machinery by these stimuli is poorly understood. Here, we show that pyruvate dehydrogenase kinase 4 (PDK4) is genetically required for cells to undergo rapid mitochondrial fragmentation when challenged with ETC toxins. Moreover, PDK4 overexpression was sufficient to promote mitochondrial fission even in the absence of mitochondrial stress. Importantly, we observed that the PDK4-mediated regulation of mitochondrial fission was independent of its canonical function, i.e., inhibitory phosphorylation of the pyruvate dehydrogenase complex (PDC). Phosphoproteomic screen for PDK4 substrates, followed by nonphosphorylatable and phosphomimetic mutations of the PDK4 site revealed cytoplasmic GTPase, Septin 2 (SEPT2), as the key effector molecule that acts as a receptor for DRP1 in the outer mitochondrial membrane to promote mitochondrial fission. Conversely, inhibition of the PDK4-SEPT2 axis could restore the balance in mitochondrial dynamics and reinvigorates cellular respiration in mitochondrial fusion factor, mitofusin 2-deficient cells. Furthermore, PDK4-mediated mitochondrial reshaping limits mitochondrial bioenergetics and supports cancer cell growth. Our results identify the PDK4-SEPT2-DRP1 axis as a regulator of mitochondrial function at the interface between cellular bioenergetics and mitochondrial dynamics.

pyruvate dehydrogenase kinase 4 | mitochondrial fission | dynamin-related protein 1 | septin 2 | OCR

Mitochondria are cellular powerhouses ubiquitously needed in healthy tissues, and they are burdened with a vast array of metabolic functions to maintain cellular integrity and function. Mitochondrial morphology is uniquely linked to its functions, including the production of adenosine triphosphate (ATP) by oxidative phosphorylation (OXPHOS) (1), cellular signaling, calcium homeostasis, regulation of programmed cell death, and maintaining the delicate balance between generation and control of reactive oxygen species (ROS). which are intricately controlled by the dynamic events of fusion and fission of the outer and inner membranes of the mitochondria (OMM and IMM) (2, 3). However, unopposed fission due to sustained nutrient excess and cellular dysfunction causes excessive mitochondrial fragmentation, a feature observed in metabolic diseases, cancer, cardiovascular and neurological disorders as well as in diseases associated with mitochondrial DNA mutations (4, 5). On the other hand, mitochondrial fusion is considered to promote OXPHOS for efficient ATP production and to allow for the biodistribution of fatty acids for fuel utilization during nutrient-deprived conditions to maintain cellular metabolite pools (1, 6). Conversely, unopposed fusion results in a hyperfused mitochondrial network, counteracts metabolic insults to preserve cellular integrity and function, and protect against mitophagy (7, 8). While the mitochondrial ultrastructural changes in response to alterations in oxidative metabolism (9) is well-documented, it has become increasingly clear that alterations in mitochondrial morphology can also have dramatic effects on the cellular metabolism.

A central regulator of mitochondrial metabolic flexibility activated by a plethora of metabolic stress is the pyruvate dehydrogenase kinases (PDKs), a family comprising of four distinctly expressed and functional kinases, PDK1 to PDK4 (10, 11). Competition between fatty acids and glucose for oxidation occurs at the level of the pyruvate dehydrogenase complex (PDC). The PDC is normally active in most tissues in the fed state and suppressing PDC activity by PDKs is crucial to maintain energy homeostasis under extreme nutritional statuses in mammals. Evidence accumulated over the past several decades has established that the loss of dynamic regulation of the PDC contributes to mitochondrial dysfunction in metabolic diseases (11). Recently, we have

Significance

Sustained energy stress and cellular dysfunction can cause excessive mitochondrial fragmentation, a feature observed in metabolic diseases, cancer, cardiovascular and neurological disorders, as well as in diseases associated with mitochondrial DNA mutations. We now show that pyruvate dehydrogenase kinase 4 (PDK4), plays a role in the regulation of mitochondrial dynamics. PDK4 promotes mitochondrial fission via phosphorylation of Septin 2 (SEPT2) at Ser^{218} and thereby triggering the recruitment of DRP1 to the mitochondria. A high level of PDK4 protein expression and SEPT2 phosphorylation was also found to be associated with lung adenocarcinoma patients with extensive mitochondrial damage. Our findings provide a mechanistic understanding that PDK4 can affect mitochondrial dynamics and cellular respiratory status under energy stress conditions.

Author contributions: T.T., D.C., J.-H.J., and I.-K.L. designed research; T.T., D.C., I.S.S., B.-G.K., M.-J.K., C.J.O., J.Y.L., and J.Y.M. performed research; B.-G.K., C.J.O., J.Y.L., Min-Ji Kim., S.Y.P., S.Y.L., M.-K.J., J.Y.M., N.I., and J.-H.J. contributed new reagents/analytic tools; T.T., D.C., B.-G.K., M.-J.K., Min-Ji Kim, J.Y.M., R.A.H., N.I., J.-H.J., and I.-K.L. analyzed data; and T.T., D.C., J.-H.J., and I.-K.L. wrote the paper.

The authors declare no competing interest.

This article is a PNAS Direct Submission.

[1]T.T. and D.C. contributed equally to this work.

[2]To whom correspondence may be addressed. Email: leei@knu.ac.kr or jeonjh@knu.ac.kr.

This article contains supporting information online at http://www.pnas.org/lookup/suppl/doi:10.1073/pnas.2120157119/-/DCSupplemental.

Published August 15, 2022.

reported that PDK4 is associated to mitochondria-associated endoplasmic reticulum (ER) membrane (MAM) formation through its direct interacts and stabilization of the mitochondrial Ca^{2+} channeling IP3R1-GRP75-VDAC1 complex (12) which promotes Ca^{2+} uptake. ER tubules have been found to wrap around mitochondria, and the MAM contact points mark the sites for fission initiation (13), a phenomenon conserved in both yeast and mammals. Although MAM formation has been implicated to promote fission and mitochondrial dynamics is known to respond to alterations in cellular metabolism, the molecular underpinnings of how changes in cellular bioenergetics and nutrient status couple to the fission and fusion machinery remain poorly understood (14). This led us to hypothesize that PDK4 might play critical role in the regulation of mitochondrial dynamics.

Results

PDK4 Induces Mitochondrial Fragmentation. We initially examined the contribution of PDK4 toward dynamic response of mitochondria when challenged with mitochondrial toxins. To this end, we generated murine embryonic fibroblast cells (MEFs) from wild-type mouse (denoted as $Pdk4^{+/+}$) and Pdk4 global knockout mice (denoted as $Pdk4^{-/-}$). MEFs were exposed to the electron transport chain (ETC) complex I inhibitor, rotenone (Rot), or complex III inhibitor, antimycin A (AMA), for 1 h. Mitochondrial morphology was assessed using endogenous TOM20 staining via confocal microscopy. Analysis of these images revealed extensive fragmentation of mitochondria caused by both the inhibitors in $Pdk4^{+/+}$ MEFs (Fig. 1 *A* and *B*). Furthermore, we performed time-lapse microscopic imaging with MitoTracker dye to visualize dynamic changes in mitochondrial morphology. This revealed a significant change in mitochondrial morphology, as visualized by extensive mitochondrial fragmentation within 15 min after the addition of rotenone (Fig. 1*C* and Movies S1 and S2). Interestingly, in comparison to the $Pdk4^{+/+}$ MEFs, mitochondrial fragmentation was significantly less dramatic in $Pdk4^{-/-}$ MEFs (Fig. 1 *A* and *B*), as visualized by TOM20 staining at fixed time points (Fig. 1*A*) and by time-lapse microscopy (Fig. 1*C* and Movies S3 and S4). Furthermore, $Pdk4^{-/-}$ MEFs demonstrated a delayed response to mitochondrial stress-induced fragmentation (Fig. 1*C*). In congruence, $Pdk4^{-/-}$ MEFs showed a significant increase in oxygen consumption rates (OCR) in comparison to the $Pdk4^{+/+}$ MEFs (Fig. 1*D*). Adenoviral overexpression was used to transiently reconstitute a wild-type PDK4 cDNA into the $Pdk4^{-/-}$ MEFs to confirm that the loss of mitochondrial fragmentation was not an artifact of the $Pdk4^{-/-}$ MEFs. In $Pdk4^{+/+}$ MEFs treated with rotenone and antimycin A, reconstituted PDK4 was sufficient to restore mitochondrial fragmentation and lower OCR, suggesting that PDK4 is capable of mediating these responses in MEFs (Fig. 1 *A*, *B*, and *D*). This indicates that increase in PDK4 level can spontaneously induce mitochondrial fragmentation even in the absence of mitochondrial inhibitors.

The well-established canonical function of PDK4 (and other PDKs, mostly PDK1 and PDK2) is to induce inhibitory phosphorylation on the PDHE1α subunit of the PDC complex (10). This inhibitory phosphorylation leads to reduced mitochondrial function which can be functionally assessed by measuring the OCR. We took into consideration the potential crosstalk between OXPHOS and mitochondrial dynamics and measured OCR in parallel with mitochondrial morphological changes pertaining to modulation of PDK isoforms. Therefore, initially, we transduced $Pdk4^{+/+}$ MEFs with adenoviruses – mock, PDK1 or PDK4 (*SI Appendix*, Fig. S1*A*). Interestingly, only PDK4-overexpressing cells demonstrated a robust fragmented pattern of the mitochondria, suggesting that mitochondrial fragmentation might be a PDK4-specific phenomenon. Next, to investigate in detail the effect of other PDK isoforms on mitochondrial dynamics, siRNA transfection was used to knockdown each of the four PDK isoforms individually in $Pdk4^{+/+}$ MEFs (*SI Appendix*, Fig. S1*B*). Unlike *Pdk4* depletion, knockdown of either *Pdk1, Pdk2* or *Pdk3* failed to reverse the effect of rotenone on mitochondrial fragmentation (*SI Appendix*, Fig. S1 *C* and *D*), suggesting that PDK4 is the critical and only PDK isoform that is involved in the regulation of mitochondrial dynamics. Interestingly, among the PDK isoforms, only PDK4 knockdown affected the canonical pathway which culminated in enhanced OCR (*SI Appendix*, Fig. S1*E*). This indicates that only PDK4 among the PDK isoforms play a critical role in regulating mitochondrial dynamics to affect cellular respiration.

To further evaluate the contribution of the canonical pathway in these two aspects of mitochondrial biology, we next used CRISP/Cas9 to genetically disrupt the PDHA1 subunit (gene that encodes PDHE1α of the PDC) in wildtype MEFs (sg*Pdha1*) (*SI Appendix*, Fig. S1*F*). Initially, we have observed that the absence of PDK4 significantly retards the stress-induced mitochondrial fragmentation process (Fig. 1 *A*–*C*). Now, we observed that in comparison to the wild-type (sgCtrl) cells, *Pdha1*-deficient cells exhibited no significant difference in the mitochondrial fragmentation pattern upon rotenone treatment (Fig. 1 *E* and *F*). To reconfirm our findings, we transiently knockdown *Pdha1* (using siRNA targeted against PDHE1α) in $Pdk4^{-/-}$ MEFs (*SI Appendix*, Fig. S1*G*). Consistent with the sg*Pdha1* cells, there was no significant difference in the effect of rotenone in the absence or presence *Pdha1* in these cells (*SI Appendix*, Fig. S1 *H* and *I*). However, as expected, *Pdha1* depletion significantly suppressed OCR in $Pdk4^{-/-}$ MEFs (*SI Appendix*, Fig. S1*J*). These results reasserted the hypothesis that the proposed noncanonical arm of PDK4 action is functionally independent of its PDHE1α regulation.

Next, to investigate the molecular details underlying the PDK4-mediated regulation mitochondrial dynamics, we challenged $Pdk4^{+/+}$ and $Pdk4^{-/-}$ MEFs with mitochondrial stressors. Treatment with either rotenone or antimycin A led to a rapid reduction of the well-established mitochondrial fusion proteins such as mitofusin (MFN) 1 and 2, and OPA1 within 30 min (*SI Appendix*, Fig. S2*A*). However, an activating (Ser^{616}) or an inhibitory (Ser^{637}) phosphorylation site of the dynamin-related protein 1(DRP1), which corresponds to regulation of DRP1-dependent mitochondrial fission (15) remained unchanged in $Pdk4^{+/+}$ and $Pdk4^{-/-}$ MEFs (*SI Appendix*, Fig. S2*B*). Similarly, no significant difference was observed in the PDHA1 phosphorylation status in $Pdk4^{+/+}$ and $Pdk4^{-/-}$ MEFs (*SI Appendix*, Fig. S2*A*), confirming our hypothesis that canonical PDK4 action doesn't contribute toward the regulation of mitochondrial dynamics. Although, no difference was observed in the expression pattern of these proteins between $Pdk4^{+/+}$ and $Pdk4^{-/-}$ MEFs, in the presence of mitochondrial stress, DRP1 localization in the mitochondria was significantly lower in the $Pdk4^{-/-}$ MEFs (Fig. 1*G*). This correlates with our earlier observations that absence of *Pdk4* ablation is associated with an elongated mitochondrial morphology (Fig. 1*A*). Mitochondrial fission involves the recruitment of DRP1 from the cytosol to the mitochondrial outer membrane (OMM) to catalyze fission reaction and this recruitment of DRP1 is aided by

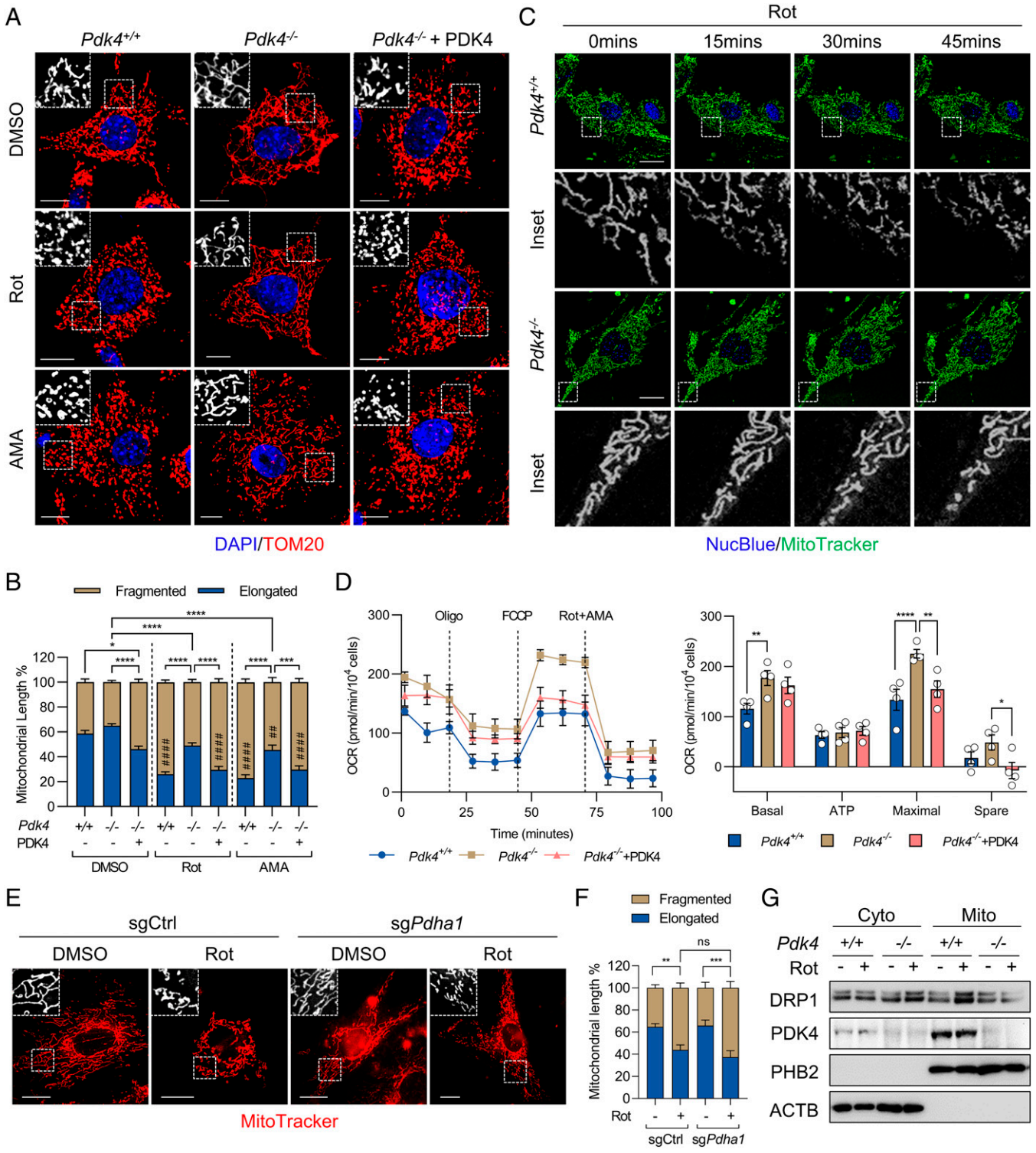

Fig. 1. PDK4 mediates energy stress-induced mitochondrial fission. (*A*) Representative confocal images of the mitochondrial morphology of wild-type (*Pdk4*$^{+/+}$) or *Pdk4* KO (*Pdk4*$^{-/-}$) MEFs, transduced with an adenovirus overexpressing PDK4 or mock control, and treated for 1 h with vehicle (DMSO), 1 μM of rotenone (Rot), or 10 μM antimycin A (AMA). Mitochondria and nucleus were visualized using an antibody to TOM20 and DAPI, respectively. (Scale bars, 15 μm.) (*B*) Quantification of the mitochondrial length of the cells shown in (*A*), >200 cells counted for each condition. (*C*) Time-lapse confocal images of *Pdk4*$^{+/+}$ or *Pdk4*$^{-/-}$ MEFs stained with MitoTracker Green and NucBlue. The indicated treatment was started at 0 min. A magnification of a portion of the mitochondrial network (dotted square) is included for each image. (Scale bars, 20 μm.) (*D*) OCR of *Pdk4*$^{+/+}$, *Pdk4*$^{-/-}$, and *Pdk4*$^{-/-}$ MEFs transduced with an adenovirus overexpressing PDK4 or mock control. (*E*) Representative confocal images of the mitochondrial morphology of wild-type (sgCtrl) or *Pdha1* KO (sg*Pdha1*) MEFs treated with DMSO or 1 μM Rot for 1 h. Mitochondria were stained with MitoTracker deep red. (Scale bars, 20 μm.) (*F*) Quantification of the mitochondrial length of the cells shown in (*E*), >100 cells counted for each condition. (*G*) Immunoblot analysis of indicated proteins in the subcellular fractions (Cyto: cytosolic fraction; Mito: mitochondrial fraction) of *Pdk4*$^{+/+}$ or *Pdk4*$^{-/-}$ MEFs treated with DMSO or 1 μM Rot for 1 h. Data are shown as the mean ± SEM of at least three independent experiments. *$P < 0.05$; **$P < 0.01$; ***$P < 0.001$; ****$P < 0.0001$, $^{\#\#}P < 0.01$; $^{\#\#\#\#}P < 0.0001$ (DMSO treated *Pdk4*$^{+/+}$ vs. Rot/AMA treated samples) by two-way ANOVA using Tukey's multiple comparison test.

several adaptor proteins residing on the surface of the mitochondria (16). However, we failed to observe any change in the expression pattern of these well-documented DRP1 adaptors (FIS1, FUNDC1, MFF, or MID49) upon rotenone treatment in $Pdk4^{+/+}$ and $Pdk4^{-/-}$ MEFs (*SI Appendix*, Fig. S2*C*), suggesting that PDK4 may directly regulate some other component(s) of the fission machinery to mediate DRP1-dependent mitochondrial fragmentation.

SEPT2 is a Conserved Substrate of PDK4. To screen for mitochondrial substrates of PDK4, we used the stable isotope labeling by amino acids in cell culture (SILAC) analysis in immortalized mouse myoblast C2C12 cell line transduced with adenoviral vectors expressing PDK4 or mock virus (Fig. 2*A* and *SI Appendix*, S2*D*). We generated a database of proteins enriched in the mitochondria upon PDK4 overexpression and performed bioinformatics analysis of the generated data (Fig. 2 *B* and *C*). This analysis identified Septin 2 (SEPT2) as a potential component of the mitochondrial fission machinery which was highly enriched as well as phosphorylated upon PDK4 overexpression (Fig. 2*C* and *SI Appendix*, Fig. S2*E*). Septins are conserved eukaryotic GTP-binding proteins and are a part of the cytoskeleton components where they can form nonpolar filaments. Mammalian septins (comprised of four subgroups: septin 2, septin 3, septin 6, septin 7) form hetero-polymeric complexes with the ubiquitously expressed SEPT2 which is present at the heart of the complexes (17). Although, in contrast to actin filaments and microtubules, septins have not been observed to interact extensively with mitochondria, a recent report has demonstrated that SEPT2 directly interacts with DRP1 and genetic ablation of SEPT2 hinders efficient localization of DRP1 at the mitochondria, thus introducing a new adaptor protein in the mitochondrial dynamics milieu (18). Our phospho-proteomic analysis revealed enhanced SEPT2 localization in the mitochondria upon PDK4 overexpression. SEPT2 contains a predicted candidate PDK4 phosphorylation site, Ser^{218} which is conserved in humans and rodents (Fig. 2 *D* and *E*). Immunoprecipitation of endogenous PDK4 resulted in coprecipitation of endogenous SEPT2 (Fig. 2*F*), indicating in vivo association of PDK4 and SEPT2. SEPT2 was directly phosphorylated by endogenous PDK4, and this phosphorylation was restored in $Pdk4^{-/-}$ MEFs upon reconstitution of PDK4 (Fig. 2*G*). Phosphorylation of SEPT2 by PDK4 was fully attenuated upon mutation of Ser^{218} (Fig. 2 *H* and *I*), as observed using a phosphomotif antibody.

To examine endogenous SEPT2 phosphorylation, we developed a phosphospecific antibody directed to phospho-Ser^{218} (pS218). SEPT2 was directly phosphorylated by recombinant PDK4, and mutation of S218 completely attenuated the in vitro phosphorylation (Fig. 2*J*). Furthermore, in the presence of mitochondrial stress, phosphorylated SEPT2 was detected exclusively in the mitochondria and this phosphorylation was significantly lower in $Pdk4^{-/-}$ MEFs (*SI Appendix*, Fig. S2*F*). To next ascertain whether the antibody to pS218 recognized mutant SEPT2 constructs when cotransfected with PDK4 cDNA, Hemagglutinin-tagged variants of SEPT2 cDNA were transiently transfected into AD-293 cells. Cotransfection with FLAG-tagged PDK4 increased reactivity of the antibody with wild-type SEPT2 phosphorylation but not with the phosphomutant (Fig. 2*K*). Additionally, SEPT2 phosphorylation by endogenous PDK4 was reduced in $Pdk4^{-/-}$ MEFs and reconstitution of PDK4 restored this effect (Fig. 2*L*). Proximity ligation assay (PLA) further confirmed the interaction of SEPT2 with PDK4 and DRP1, and localization of PDK4-SEPT2 and SEPT2-DRP1 blobs at the mitochondrial fission sites (Fig. 2*M*), thus indicating a potential axis involving PDK4-SEPT2-DRP1 to play a role in regulating mitochondrial dynamics.

PDK4-Induced $SEPT2^{S218}$ Phosphorylation is Required for Recruitment of DRP1 to the Mitochondria. To test the effects of PDK4 phosphorylation on SEPT2 function, we first used MEFs that have been reported previously as lacking the most well-documented DRP1 receptors ($Mff^{-/-}$, $Fis1^{-/-}$, $Mid49^{-/-}$, and $Mid51^{-/-}$ denoted as QKO MEFs) (19) (Fig. 3*A*). In comparison to the wild-type cells, QKO MEFs demonstrated an elongated mitochondrial morphology. However, forced overexpression of PDK4 induced significant amount of mitochondrial fragmentation in QKO MEFs, and this was abolished upon siRNA-mediated knockdown of SEPT2 (Fig. 3 *B* and *C*), indicating that SEPT2 ablation is necessary to mitigate PDK4-induced mitochondrial fission. Subsequent analysis of subcellular fractions in QKO MEFs further revealed that SEPT2 knockdown hinders efficient recruitment of DRP1 to the mitochondria by PDK4 (Fig. 3*D*). Furthermore, mitochondrial stress-induced fragmentation in QKO MEFs was significantly attenuated upon knockdown of SEPT2, thus confirming the dependency on PDK4-SEPT2 axis in this MEFs to undergo mitochondrial fission even in the absence of the known DRP1 receptors (*SI Appendix*, Fig. S3 *A–C*). This observation signifies the importance of PDK4-SEPT2 axis as a crucial mediator of mitochondrial stress-induced fragmentation.

Next, to validate that the PDK4-SEPT2 axis mediates its effect through DRP1, we used MEFs that were genetically disrupted for DRP1 (denoted as $Drp1^{-/-}$) to evaluate the effect on mitochondrial dynamics (*SI Appendix*, Fig. S3*D*). Consistent with previous observations that DRP1 is an indispensable component for mitochondrial fission machinery (20), $Drp1^{-/-}$ MEFs demonstrated a significantly fused mitochondrial morphology compared to the wild-type cells, and even forced overexpression of PDK4 failed to reverse this fused phenotype (*SI Appendix*, Fig. S3 *E* and *F*), demonstrating that DRP1 is necessary for PDK4-SEPT2-dependent mitochondrial fragmentation.

As a key adaptor for DRP1, SEPT2 is essential for steady-state localization of DRP1 to the mitochondria (18). PLA analysis demonstrated enhanced SEPT2-DRP1 interaction at the mitochondrial fission sites and increased mitochondrial fragmentation upon PDK4 overexpression (Fig. 3 *E–G*). In addition, immunofluorescence analysis revealed a significantly enhanced colocalization of endogenous DRP1 to the mitochondria upon overexpression of PDK4 in wild-type SEPT2-expressing cells, as compared with the control vector (Fig. 3 *H* and *I*). These effects were mitigated in phospho-mutant SEPT2-expressing cells (S218A-SEPT2) even in the presence of PDK4 overexpression, whereas phospho-mimic SEPT2-expressing cells (S218D-SEPT2) reversed these effects even without the requirement for PDK4 overexpression (Fig. 3 *E–I*). These observations were revalidated using subcellular fractionation assay which aligned with the immunofluorescence findings (Fig. 3*J*). Furthermore, reconstitution of $Pdk4^{-/-}$ MEFs with wild-type PDK4 revealed increased mitochondrial fragmentation (*SI Appendix*, Fig. S3 *G* and *H*) and endogenous DRP1 translocation to the mitochondria when PDK4 expression was restored (*SI Appendix*, Fig. S3*I*). Ablation of *Sept2* strongly repressed mitochondrial fragmentation (*SI Appendix*, Fig. S3 *G* and *H*) and reduced DRP1 translocation to the mitochondria in $Pdk4^{-/-}$ MEFs reconstituted with PDK4 (*SI Appendix*, Fig. S3*I*). Mitochondrial fission is associated with lowered OCR (21). Consistent with this hypothesis, SEPT2 ablation exhibited enhanced maximal and spare capacity in OCR,

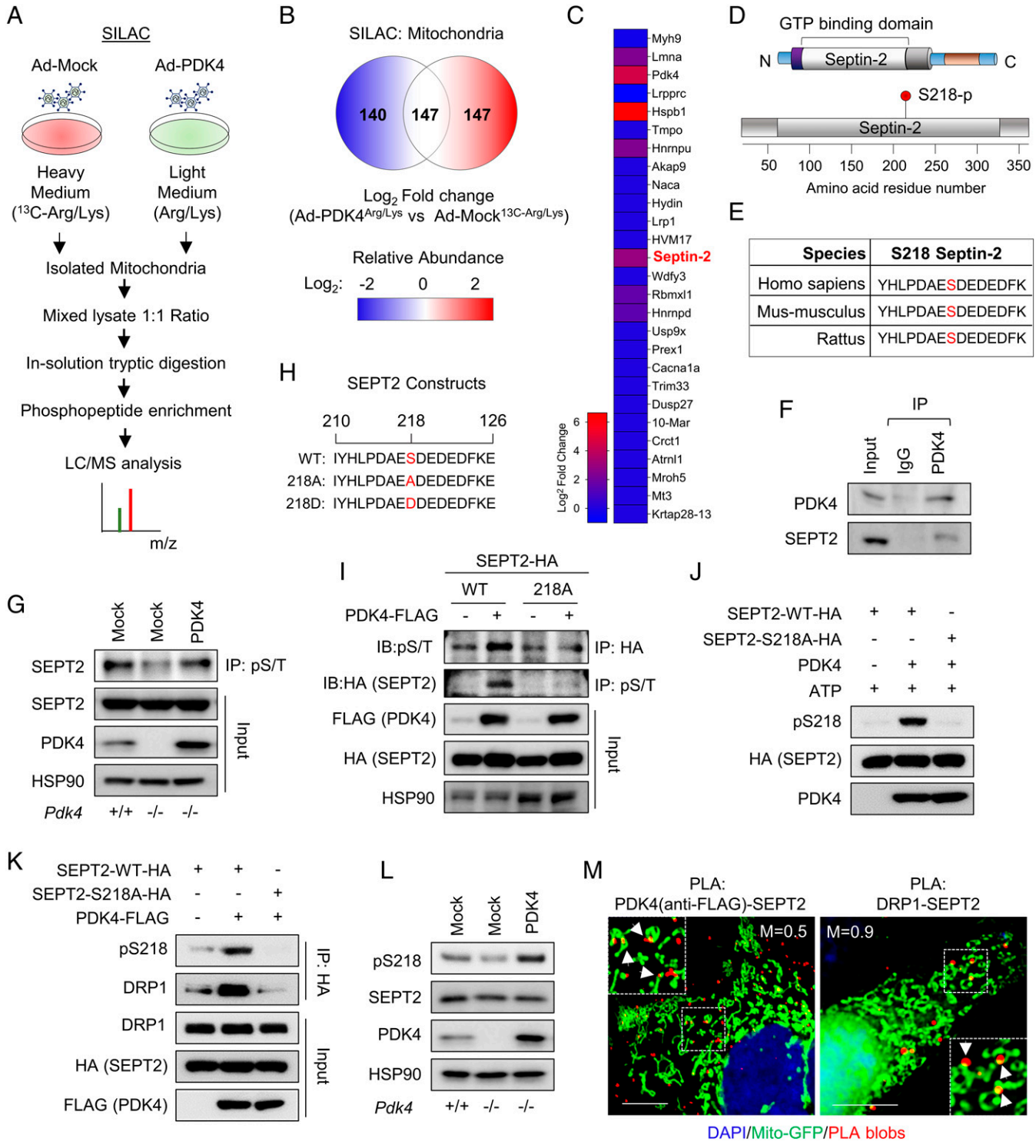

Fig. 2. PDK4 phosphorylates SEPT2 and enhances SEPT2-DRP1 interaction. (*A*) Schematic depiction of SILAC-LC-MS/MS analysis of C2C12 myoblasts transiently transduced with adenovirus (Ad)-mock or PDK4 as indicated. (*B*) Venn diagram depicting down-, unchanged- and up-regulated proteins in the mitochondrial fraction of the cells in (*A*). (*C*) Heat map showing the abundance of phosphorylated proteins in the mitochondrial fraction of the cells in (*A*). (*D*) Schematic illustration of SEPT2 domain structure and location of the PDK4 substrate motif, serine 218 (S218) relative to functionally annotated GTP-binding domain at amino terminus. (*E*) ClustalW alignment of SEPT2 amino acid sequences showing that S218 site is conserved among the mammalian species. (*F*) Coimmunoprecipitation of SEPT2 with PDK4 in *Pdk4*$^{+/+}$ MEFs. PDK4 immunoprecipitates and lysate was immunoblotted with the indicated antibodies. (*G*) Coimmunoprecipitation of SEPT2 with PDK4 in *Pdk4*$^{+/+}$ and, *Pdk4*$^{-/-}$ MEFs transduced with adenovirus-mock or PDK4. Phospho-serine/threonine (pS/T) immunoprecipitates and lysates were immunoblotted with the SEPT2 antibody. (*H*) Schematic of SEPT2 cDNA illustrating the generation of SEPT2 S218A (phospho-mutant) and S218D (phospho-mimetic) mutant construct at the location of serine 218. (*I*) AD-293 cells were cotransfected with HA-tagged WT or SEPT2 S218A mutant and empty vector (−) or PDK4-FLAG (+). HA/pS/T immunoprecipitations and total cell lysates were immunoblotted as indicated. (*J*) Immunoblot analysis of in vitro kinase assay of recombinant PDK4 protein and SEPT2 WT or S128A Immunoprecipitates. (*K*) AD-293 cells cotransfected with HA-tagged WT or SEPT2 S218A mutant and empty vector (−) or PDK4-FLAG (+). HA immunoprecipitates and lysates were immunoblotted with the indicated antibodies and phosphomotif antibody that recognizes phosphorylated SEPT2 at Ser218. (*L*) Immunoblot analysis of indicated proteins in *Pdk4*$^{+/+}$ and, *Pdk4*$^{-/-}$ MEFs transduced with adenovirus-mock or PDK4. Phosphorylation of endogenous SEPT2 was detected by the antibody specific to SEPT2 Ser218. (*M*) Protein-protein interactions between SEPT2 and PDK4/DRP1 were visualized by Proximity Ligation Assay (PLA) in AD-293 cells transiently transfected with PDK4-FLAG (*Left*) or endogenous DRP1 (*Right*) using anti-SEPT2 and anti-FLAG or anti-DRP1 antibodies. Predominantly, PLA blobs were observed on the mitochondrial fission sites (arrows). Magnified portion of the mitochondrial network (dotted square) is included for each image. Manders' coefficient (M) indicates fraction of PLA blobs overlapping mito-GFP. (Scale bars, 10 μm.).

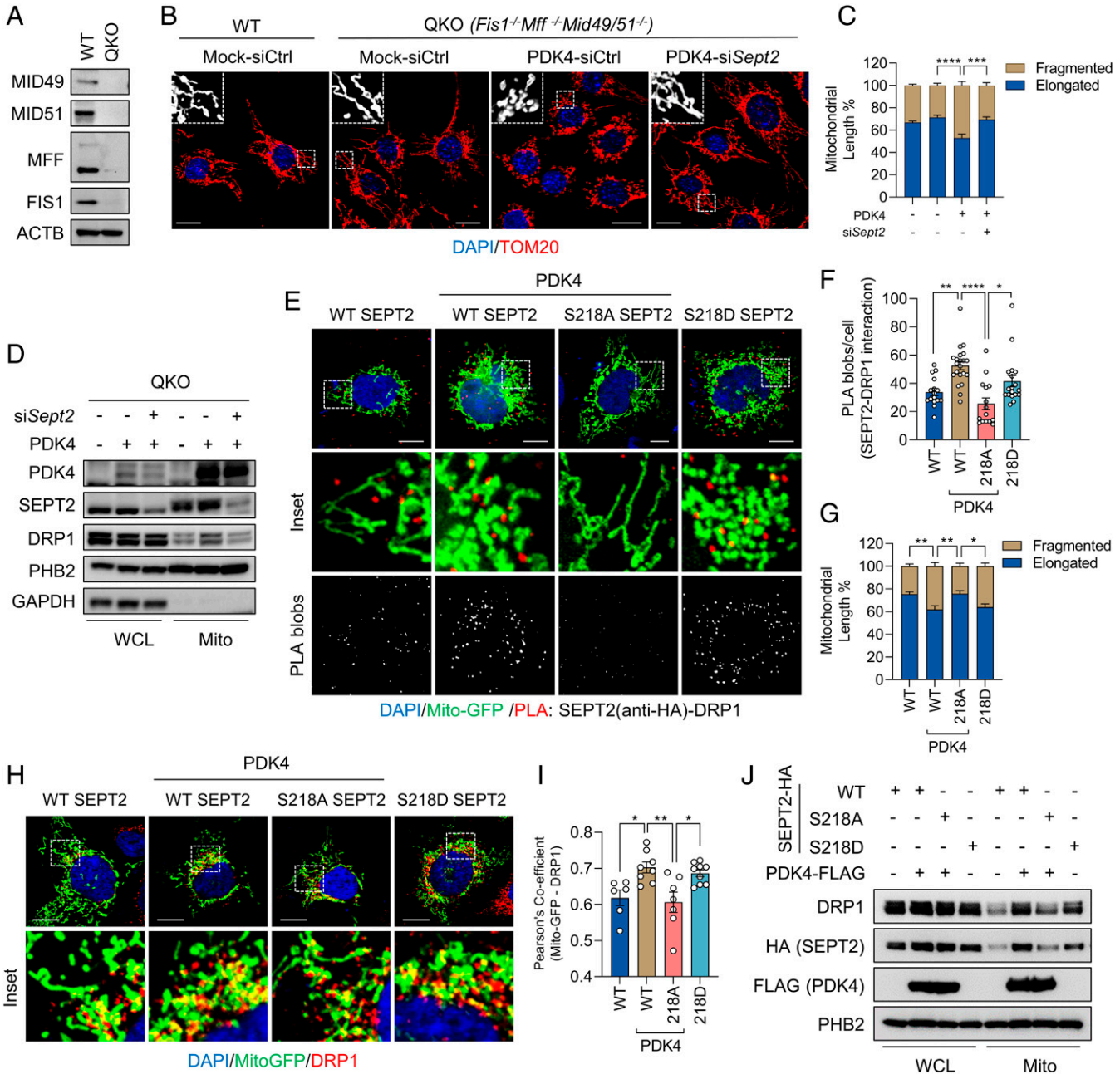

Fig. 3. PDK4-dependent SEPT2 phosphorylation is critical for DRP1 recruitment to the mitochondria. (*A*) Immunoblot analysis of indicated proteins in WT or QKO (*Mff*$^{-/-}$*Fis1*$^{-/-}$*Mid49/51*$^{-/-}$) MEFs. (*B*) Representative confocal images of the mitochondrial morphology of WT and QKO MEFs, transduced with an adenovirus overexpressing PDK4 or mock control, after transient knockdown of *Septin2* using siRNA (si*Sept2*). Mitochondria and nucleus were visualized using an antibody to TOM20 and DAPI, respectively. (Scale bars, 20 μm.) (*C*) Quantification of the mitochondrial length of the cells shown in (*B*). (*D*) Immunoblot analysis of indicated proteins in the subcellular fractions (WCL: whole cell lysate; Mito: mitochondrial fraction) of WT or QKO MEFs, transduced with adenovirus-mock (−) or PDK4 (+), after transient knockdown of *Septin2* using siRNA (si*Sept2*) (+) or siCtrl (−). (*E*) DRP1 and exogenous SEPT2 interaction were visualized by PLA using anti-HA and anti-DRP1 antibodies in AD-293 cells ectopically expressing HA-tagged WT, SEPT2 S218A, or SEPT2 S218D mutants and PDK4-FLAG together with a plasmid encoding for mitochondrial-targeted GFP (mito-GFP). (Scale bars, 10 μm.) (*F*) Quantification of the PLA blobs of the cells shown in (*E*). (*G*) Quantification of the mitochondrial length of the cells shown in (*E*). (*H*) DRP1 recruitment to the mitochondria were visualized by immunofluorescence (IF) using anti-DRP1 antibody in AD-293 cells ectopically expressing HA-tagged WT, SEPT2 S218A, or SEPT2 S218D mutants and PDK4-FLAG together with a plasmid encoding for mitochondrial-targeted GFP (mito-GFP). (Scale bars, 15 μm.) (*I*) Quantification of the colocalization between mito-GFP and DRP1 of the cells shown in (*H*). (*J*) Immunoblot analysis of indicated proteins in the subcellular fractions (WCL: whole cell lysate; Mito: mitochondrial fraction) of AD-293 cells transiently transfected with HA-tagged WT, SEPT2 S218A, or SEPT2 S218D mutants and PDK4-FLAG as indicated. Data are shown as the mean ± SEM of at least three independent experiments with >200 cells counted for each condition. **P* < 0.05; ***P* < 0.01; ****P* < 0.001; *****P* < 0.0001 by ordinary one-way or two-way ANOVA using Tukey's multiple comparison test.

comparable to *Pdk4*$^{-/-}$ MEFs, even after PDK4 reconstitution (*SI Appendix*, Fig. S3*J*). These data indicate that conditions which activate PDK4 can induce acute DRP1 translocation to mitochondria and affect cellular bioenergetics, and this effect is abolished when PDK4 cannot phosphorylate Ser^{218} in SEPT2.

Suppression of PDK4-SEPT2 Axis Improves Mitochondrial Dynamics and Function in *Mfn2*-Deficient Cells. The mitofusin family of proteins (MFN1 and MFN2) positively mediate mitochondrial fusion by merging the outer membranes of the mitochondria (2, 3). Genetic mutations of *Mfn2* lead to

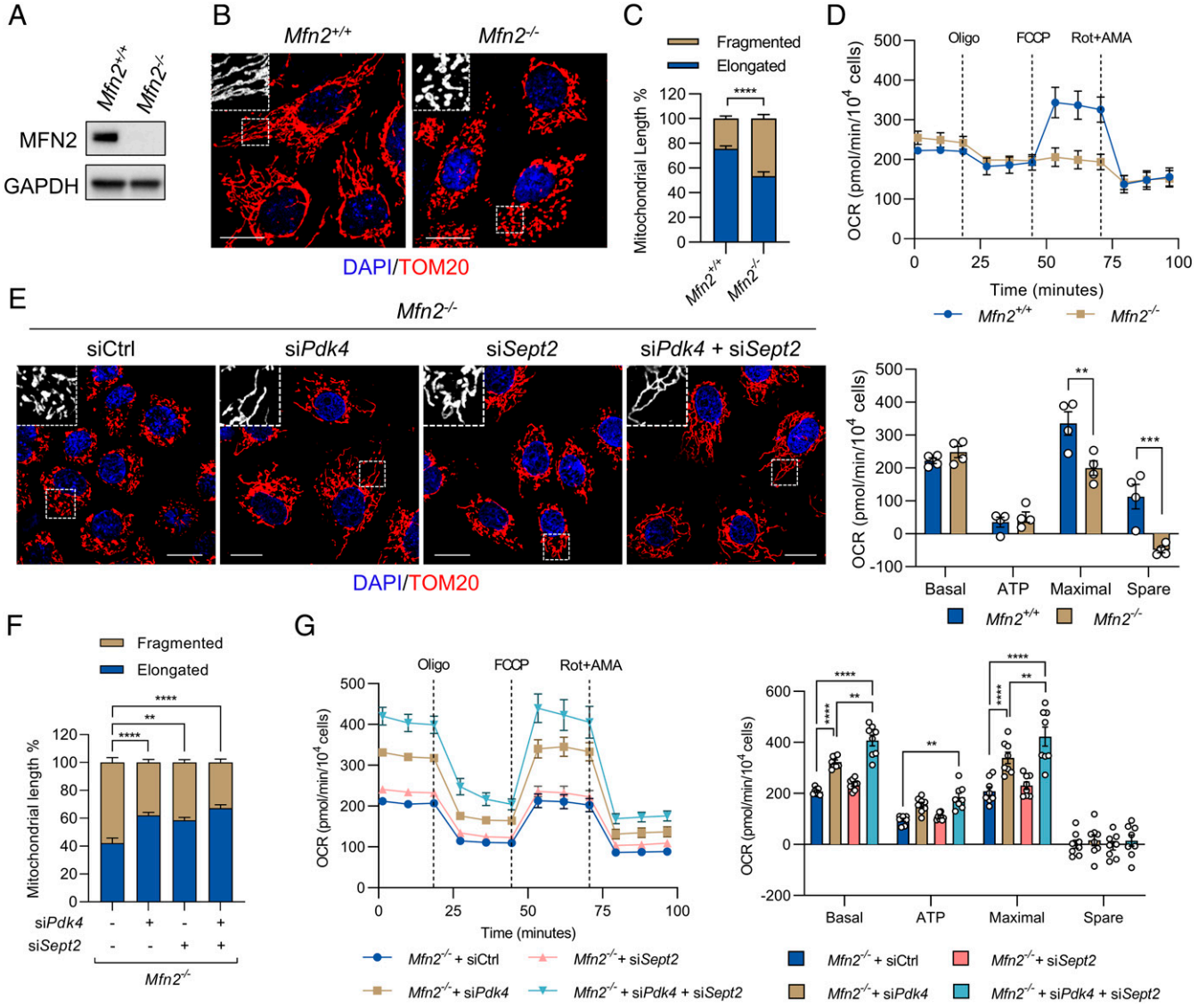

Fig. 4. Inactivation of PDK4-SEPT2 axis corrects mitochondrial dynamics and function in *Mfn2* deficient cells. (*A*) Immunoblot analysis of indicated proteins in wild-type ($Mfn2^{+/+}$) or *Mfn2* KO ($Mfn2^{-/-}$) MEFs. (*B*) Representative confocal images of the mitochondrial morphology of $Mfn2^{+/+}$ or $Mfn2^{-/-}$MEFs. Mitochondria were visualized using an antibody to TOM20. (Scale bars, 20 μm.) (*C*) Quantification of the mitochondrial length of the cells shown in (*B*). (*D*) OCR of the cells shown in (*B*). (*E*) Representative confocal images of the mitochondrial morphology of $Mfn2^{-/-}$ MEFs transiently transfected with control (Ctrl), *Pdk4* or *Sept2* siRNAs for 48 h. Mitochondria were visualized using an antibody to TOM20. (Scale bars, 20 μm.) (*F*) Quantification of the mitochondrial length of the cells shown in (*E*). (*G*) OCR of the cells shown in (*E*). Data are shown as the mean ± SEM of at least three independent experiments with >200 cells counted for each condition. $^{**}P < 0.01$; $^{**}P < 0.01$; $^{***}P < 0.001$; $^{****}P < 0.0001$ by two-way ANOVA using Tukey's/Sidak's multiple comparison test.

unopposed mitochondrial fission in the most common inheritable axonal neuropathy-related Charcot-Marie-Tooth disease type 2A (CMT2A) (22). However, mitofusin agonist treatment can correct this dominant suppression of mitochondrial fusion by these disease-causing mutations (23). Therefore, we evaluated the concept of suppressing mitochondrial fission to restore balance in mitochondrial dynamics in *Mfn2* knockout ($Mfn2^{-/-}$) MEFs (Fig. 4*A*). Expectedly, $Mfn2^{-/-}$ MEFs demonstrated significantly higher amount of mitochondrial fragmentation (Fig. 4 *B* and *C*) and lower levels of OCR (Fig. 4*D*) compared to $Mfn2^{+/+}$ MEFs. Knockdown of either *Pdk4* or *Sept2* or dual knockdown led to a reversal of this phenotype, as observed from enhanced mitochondrial fusion (Fig. 4 *E* and *F*). Furthermore, *Pdk4* or dual knockdown of *Pdk4* and *Sept2*, but not *Sept2* knockdown alone, improved the OCR levels in $Mfn2^{-/-}$ MEFs (Fig. 4*G*), indicating that PDK4 can regulate mitochondrial bioenergetics, at least in part, by mechanisms independent of SEPT2. However, *Pdk4*, *Sept2* or the dual knockdown failed to have any observable effect on mitochondrial fusion upon genetic ablation of the complete mitochondrial outer membrane fusion machinery in $Mfn1/2^{-/-}$ MEFs (*SI Appendix*, Fig. S4 *A*–*C*), supporting earlier observations that MFN1 can compensate for MFN2 deficiency (24). These findings add a further layer of regulation in balancing mitochondrial fission-fusion by suggesting that in MFN2 dysfunctional or deficient status, targeting mitochondrial fission can restore the balance toward optimal mitochondrial dynamics.

PDK4-SEPT2 Pathway Mediates Mitochondrial Fission to Promote Cancer Cell Proliferation. Hypoxia is a nutrient-deprived stress condition where cells adapt to their microenvironment via a number of mechanisms, including alteration of mitochondrial bioenergetics and dynamics, leading to enhanced mitochondrial fragmentation (25, 26). Initially, we investigated whether PDK4-dependent mitochondrial fission occurs in this environmental stress condition. Transient hypoxia-induced mitochondrial fission and DRP1-SEPT2 interaction was significantly

mitigated upon *PDK4* ablation in human proximal tubular HK2 cells (*SI Appendix*, Fig. S5 *A–C*). Next, to further evaluate the function of the PDK4-dependent phosphorylation of SEPT2 in vivo, in a tumor type in which PDK4 pathway is activated (27) and in which mitochondrial homeostasis in critical (28), we investigated whether stimulated PDK4-dependent mitochondrial fission occurs in human lung adenocarcinoma by immunoblotting the lysates of tumor and nontumor biopsy samples from ten patients. Seven of 10 (*SI Appendix*, Table S1) individual tumors (T) exhibited high expression of PDK4 and SEPT2 phosphorylation compared to adjacent nontumor (N) tissue (Fig. 5*A*). Electron microscopic analysis revealed extensive mitochondrial fragmentation and enhanced mitochondrial circularity in the tumor tissue (Fig. 5 *B* and *C*). Consistently, depletion of PDK4 in two lung adenocarcinoma cell lines (H460 and Calu-3) suppressed SEPT2 phosphorylation (Fig. 5*D*) and interaction with DRP1 (Fig. 5 *E* and *F*), reduced mitochondrial fragmentation (Fig. 5 *G* and *H*), decreased extracellular acidification rates (Fig. 5 *I* and *J*) and suppressed spheroid formation in these cells (Fig. 5 *K* and *L*). These results indicate that the PDK4-SEPT2-DRP1 axis promotes mitochondrial fission and facilitates tumor growth in lung adenocarcinoma (Fig. 5*M*).

Discussion

Morphologically, mitochondria vary widely across cell types and tissues and respond rapidly to cellular insults and metabolic cues, such as nutrient and energy status (1). Balanced fusion and fission events, termed as mitochondrial dynamics, shapes the mitochondria to attain cellular metabolic demands and to ensure mitochondrial quality control (MQC) through removal of damaged organelles (4, 29). Under physiological conditions, stress-induced mitochondrial damage and fission initiates a cellular adaptive mechanism which leads to degradation and the autophagic clearance of defective mitochondrial sectors (mitophagy) or apoptosis under severe conditions (29). This facilitates physical segregation and proper functioning of the still-intact mitochondrial elements. PDKs show unique tissue expression patterns, kinetic properties and sensitivities to regulatory molecules. Despite its low basal expression, PDK4 is dramatically increased in tissues challenged with stressful stimuli, including in cisplatin-challenged renal tissue (30), high inorganic phosphate-treated vascular smooth muscle cells (31), and diabetes in liver, heart, and skeletal muscle (32, 33). Given that these pathological conditions give rise to mitochondrial dysfunction, as evidenced by mitochondrial ROS formation, decreased mitochondrial membrane potential (MMP) and decreased ATP production (30, 31), it is reasonable to assume PDK4 is mechanistically linked with mitochondrial dysfunction.

Mitochondrial fission, which is required for apoptosis, as well as normal cell growth and development is partly controlled by the of DRP1 phosphorylation at Ser^{616} by several kinases including Cdk1/cyclin B and MAPK/ERK2 and at Ser^{637} by protein kinase A (PKA). In addition to phosphorylation, several adaptors have been demonstrated to be required for steady-state localization of DRP1 to the mitochondria (16). Our findings indicate a distinct regulatory mode of DRP1-dependent mitochondrial fission, where SEPT2 is one of the first PDK4 substrates to have been discovered to directly control mitochondrial ultrastructure. These findings parallel an earlier report where AMPK was shown to phosphorylate a well-documented DRP1 adaptor, MFF, to promote mitochondrial fragmentation (34). Interestingly, using QKO MEFs (lacking the functional DRP1 adaptors) we observe that the PDK4-SEPT2 axis can still drive mitochondrial fission, suggesting a critical role of this axis in determining the balance in mitochondrial dynamics.

Loss of PDK4 mitigates cell growth in lung tumor cells harboring KRAS mutations (27). Interestingly, Ras-driven tumors exploit DRP1- dependent mitochondrial fragmentation to drive cancer cell growth, and inhibition of DRP1 is sufficient to block xenograft growth (35). In congruence with these observations, SEPT2 has been reported to be up-regulated in several cancer types, promoting cell migration and invasion through the MEK/ERK pathway (36). This may explain our findings that PDK4-SEPT2-DRP1 axis is a potent oncogenic driver that utilizes the mitochondrial dynamics as a conduit for cancer cell proliferation. Direct targeting of RAS is difficult, thus, there is a significant unmet need to elucidate the downstream processes that underlie its oncogenic effects. Collectively, these observations suggest that identifying new targets involved in the regulation of mitochondrial fission may make MAPK-driven malignancies amenable to therapy.

Among the PDK isoforms, PDK4 is almost invariably and exclusively up-regulated in mitochondrial dysfunction-related metabolic diseases. Mitochondria being the major source of cellular ATP, the maintenance of mitochondrial function is paramount to maintaining overall energy homeostasis (37), but the question of whether PDK4 plays direct roles in different aspects of mitochondrial biology remained unaddressed. Here, we show that PDK4 acutely triggers mitochondrial fission, at least in part via phosphorylation of SEPT2 (*SI Appendix*, Fig. S6). This rapid PDK4-dependent induction of mitochondrial fragmentation may serve as a way for the cell to prepare to initiate removal of damaged mitochondrial sectors through mitophagy, a hitherto unknown aspect which requires immediate attention. Although, PDK4 lies central to mitochondrial homeostasis, SEPT2 is one of the first PDK4 substrates to have been identified to be directly involved in mitochondrial dynamics and bioenergetics. PDK4 is known to be induced in various pathologies where the underlying pathogenesis implicates mitochondrial dysfunction as a critical initiation point. Thus, PDK4 emerges as a central player of mitochondrial homeostasis and an amenable therapeutic target in human pathologies.

In the past decades, remarkable progress has been made to identify the core elements and regulatory factors that control mitochondrial dynamics machinery in mammals. Significant efforts have led to the elucidation of the molecular underpinnings that regulate mitochondrial fission and fusion events in normal and pathological conditions (38). In that context, emerging evidence has linked mitochondrial dynamics with mitochondrial quality control via selective exclusion of damaged sectors within the mitochondria (ie, mitophagy) (39). Although PDK4 promotes mitochondrial fission, it remains to be determined precisely how PDK4 exerts its influence on the overall mitochondrial quality control process. Furthermore, association of ER with mitochondria (MAMs) have been shown to play an active role in MQC (40). Earlier, we have demonstrated that PDK4 contributes toward to MAM formation (12). However, the crosstalk between mitochondrial dynamics and MAM formation and to what extent PDK4 plays a role in promoting this crosstalk remains to be elucidated. Last, mitochondrial dynamics is closely associated with tumor formation and metastasis. Several studies have implied that DRP1/MFN exerts varied effects in different cancers (39). Therefore, a definitive conclusion about the role of PDK4 in the occurrence and metastasis of tumors in humans will require an in-depth analysis. Given that PDK4 plays a critical role in several mitochondrial processes and has been implicated in other indications related to metabolic disease (10, 11), it may be possible to test PDK4 for a potential targeted therapy based on the regulation of mitochondrial dynamics-related factors.

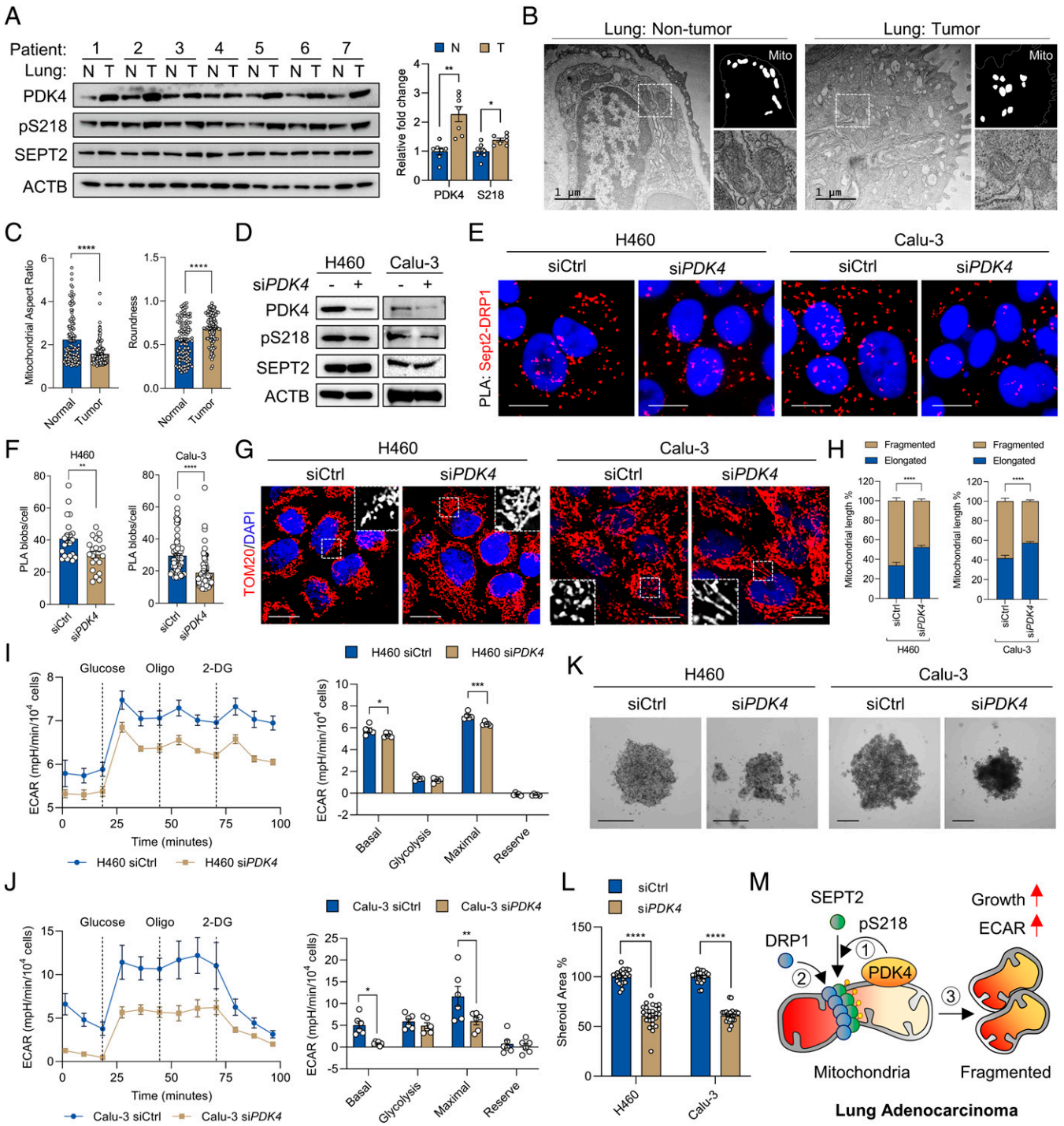

Fig. 5. Inhibition of PDK4-SEPT2 pathway limits cancer cell growth. (*A*) Immunoblot analysis of indicated proteins in tumor (T) and corresponding adjacent nontumor (N) tissue lysates from patients with lung adenocarcinoma. (*Left*) Immunoblot quantification of PDK4 and pS218 were normalized with ACTB and SEPT2, respectively. **P* < 0.05; ***P* < 0.01 by paired *t* test. (*B*) Representative transmission electron microscopic (TEM) images and analysis of mitochondrial morphology of tissue samples (patient 1 and 2) shown in (*A*). (Scale bars, 1 μm.) (*C*) Analysis of mitochondrial morphology of the TEM images shown in (*B*). (*D*) Immunoblot analysis of indicated proteins in H460 and Calu-3 cells transiently transfected with *Pdk4* siRNA for 48 h. (*E*) PLA of indicated proteins in H460 and Calu-3 cells transiently transfected with *Pdk4* siRNA for 48 h using anti-SEPT2 and anti-DRP1antibodies. (Scale bars, 15 μm.) (*F*) Quantification of the PLA blobs of the cells shown in (*E*). (*G*) Representative confocal images of the mitochondrial morphology of H460 and Calu-3 cells transiently transfected with *Pdk4* siRNA for 48 h. Mitochondria were visualized using an antibody to TOM20. (Scale bars, 15 μm.) (*H*) Quantification of the mitochondrial length of the cells shown in (*G*). (*I* and *J*) Extracellular acidification rate (ECAR) measurement of H460 (*I*) and Calu-3 (*J*) cells transiently transfected with *Pdk4* siRNA for 48 h. (*K*) Representative images of spheroid cultures of H460 and Calu-3 cells transiently transfected with *Pdk4* siRNA after 72 h. (Scale bars, 500 μm.) (*L*) Quantification of the spheroid surface area (in %) of the cells shown in (*K*). (*M*) Molecular model depicting the role of PDK4-SEPT2-DRP1 axis in regulating mitochondrial dynamics in lung tumor. Data are shown as the mean ± SEM of at least three independent experiments with >200 cells counted for each condition. Data are shown as the mean ± SEM of at least three independent experiments with >200 cells counted for each condition. **P* < 0.05; ***P* < 0.01; ****P* < 0.001; *****P* < 0.0001 by unpaired *t* test or two-way ANOVA using Sidak's multiple comparison test.

Materials and Methods

Detailed materials and methods are listed in *SI Appendix*.

Human Tissue. Lung tumor (adenocarcinoma) and adjacent nontumor lung tissue specimens from seven patients (with no history of chemotherapy) along with the clinical information of each individuals were provided by the National Biobank of Korea-Kyungpook National University Hospital; Daegu, South Korea. Detailed patient information is provided in *SI Appendix*, Table S1.

Cell Culture. Primary MEFs were isolated and cultured from *Pdk4*$^{+/+}$ and Pdk4$^{-/-}$ mice embryo on embryonic day (E) 13.5 as previously described (41) and all the experiments were performed within one to four passage number. The list of cells used for the experiments are described in *SI Appendix*, Table S2. MEFs and Calu-3 cells were cultured in DMEM media (LM001-05; Welgene) containing 10% FBS (16000-044; Gibco), 1× Pen Strep antibiotics (15140-122; Gibco). H460 and HK2 cells were cultured in RPMI (30-2001; ATCC) and RPMI (11875-093; Gibco) media, respectively, supplemented with 10% FBS (16000-044; Gibco), 1X Pen Strep antibiotics (15140-122; Gibco) in 5% CO_2 at 37 °C.

siRNAs, Plasmid Vector, and Adenovirus Constructs. Predesigned siRNAs targeting mouse *Pdk4* (#1406883), *Pdk1* (#228026-2), *Pdk2* (#18604-3), *Pdk3* (#236900-1), *Pdha1* (#18597-2), *Sept2* (#1423300), human *PDK4* (#5166-2) and siControl (#SN-1003) were purchased from Bioneer (Daejeon). Human SEPT2 plasmid DNA construct (hMU003202; KIRBB gene bank, Daejeon) was used to generate SEPT2 mutant S218A and S218D by site-directed mutagenesis technique using the QuikChange Lightning Site-Directed Mutagenesis Kit (210518-5; Agilent Technologies) and inserted in pcDNA3 plasmid vector after adding a HA tag in the C terminus. PDK4 with C terminus tagged with FLAG in pcDNA3 vector was provided Dr. Robert A. Harris (Indiana University) and PDK4 with C terminus tagged with FLAG adenovirus was provided by Dr. Y.-B. Kim (Harvard Medical School). mitochondria-targeted GFP (mito-GFP) was provided by Dr. Hyun-Woo Rhee (Seoul National University). pcDNA3 and mock adenovirus served as control for transient transfections and adenovirus transductions, respectively.

Experimental Treatments and Condition. After overnight cell plating, cells were challenged with dimethyl sulfoxide (DMSO; D2650; Sigma) as vehicle control or 1 μM Rotenone (R8875; Sigma-Aldrich) or 10 μM Antimycin A (A8674; Sigma-Aldrich) for the indicated time points. For treatment in transient knockdown or overexpressing conditions, cells were transfected with siRNA/plasmid DNA using RNAi Max reagent/LipofectamineTM 2000 (13778150/11668019; Thermo Fisher Scientific) or transduced with adenovirus for 48 h. Then, the cells were challenged with DMSO or 1 μM Rotenone or 10 μM Antimycin A for the indicated time points. For hypoxic condition, HK2 cells were plated overnight and transfected with siRNA for 48 h. Then, the cells were exposed to hypoxic condition (1% O_2) for 1 h using INVIVO$_2$ 400 (Hypoxia workstation).

Immunofluorescence Imaging. At the end of the experiment, cells were washed with PBS, fixed with 4% paraformaldehyde, permeabilized (0.2% Triton X, 0.1M glycine in PBS), and incubated with the indicated primary antibodies overnight at 4 °C. The next day, the cells were washed, incubated with the secondary antibodies conjugated with fluorophores (Alexa-488/568), and mounted using VECTASHIELD mounting medium containing DAPI (H1200). Images were taken using Olympus FluoView FV1000 confocal microscope (Olympus Imaging). Colocalization% and mitochondrial length (>10 μm considered as elongated and <10 μm considered as fragmented) were quantified using ImageJ software with Fiji plugin (NIH).

Time-Lapse Confocal Imaging. MEFs were plated on glass bottom confocal dish (100350; SPL life sciences). Before imaging, cells were prestained with NucBlue (R37605; Thermo Fisher Scientific) and MitoTracker Green (M7514; Thermo Fisher Scientific) or MitoTracker Deep Red (M22426; Thermo Fisher Scientific), washed, and replaced the medium with phenol red free-DMEM media (LM001-10). Immediately, after the addition of 1 uM Rotenone (final concentration), time-lapses images were captured and tracked for every 1 min until the indicated endpoint using confocal laser scanning microscope FV3000 (Olympus).

Subcellular Fractionation. Mitochondria and cytosolic fractions from cells/human tissue were prepared by following the manufacturer's Dounce homogenization method using mitochondria isolation kit (89874/89801; Thermo Fisher Scientific).

In Vitro Kinase Assay. In vitro kinase assay was performed as described previously (42). Briefly, AD293 cells transiently transfected with HA-SEPT2 constructs and cells were lysed 36 h after the transfection. Cell lysates were then subjected to HA-immunoprecipitation using commercially available HA-beads (26181; Thermo Fisher Scientific). Immunoprecipitates were washed with lysis buffer (3 times) followed by and additional washing steps (3 times) with the kinase buffer (9802; Cell Signaling Technology). The kinase reaction was initiated with the addition of 100 μM ATP and 2 mM DTT in the absence or presence of 50 ng active recombinant PDK4 (provided by Dr. Nam-Ho Jeoung, Catholic University). The reactions were incubated for 30 min at 30 °C and processed for downstream immunoblotting analysis.

Spheroid Formation Assay. H460 or Calu-3 Cells seeded at a density of 6×10^3 in ultra-low cluster, 96 well plate (7007; Costar), reverse transfected with control/*Pdk4* siRNA and cultured for 72h. Then, the images were captured using ImageXpress Micro confocal (Molecular Devices) and spheroid size was analyzed using MetaXpress software (Molecular Devices).

Statistical Analysis. GraphPad Prism 8 (GraphPad Software) was used for plotting graph and statistical analysis. Statistical significance analysis was performed using Student's *t* test and one-way or two-way ANOVA with recommended comparison test from at least three independent experiments specified in each figure legends. $P < 0.05$ was considered statistically significant and results are presented as mean ± SEM.

Data Availability. All data are included in the manuscript and/or supporting information. The mass spectrometry proteomics data have been deposited to the ProteomeXchange Consortium via the PRIDE partner repository with the dataset identifier PXD028379 and 10.6019/PXD028379 (43).

ACKNOWLEDGMENTS. We thank Mike Ryan and his laboratory members (Monash University), Antonio Zorzano and his laboratory members (IRB Barcelona) for providing us with knockout MEFs. This work was supported by Basic Science Research Program through the National Research Foundation of Korea (NRF) funded by the Ministry of Science and ICT (NRF-2017R1A2B3006406) and the Korea Health technology R&D Project through the Korea Health Industry Development Institute (KHIDI), funded by the Ministry of Health & Welfare, Republic of Korea. (Grant Number: HI16C1501) (to I.-K.L.); NRF grant funded by the Ministry of Science and ICT (NRF-2021R1A5A2021614 and NRF-2020R1C1C1012729) (to J.-H.J.); NRF 2021R1F1A1061393 (to D.C.); NRF 2019R1I1A1A01062408 (to T.T.); KBRI basic research program through Korea Brain Research Institute funded by Ministry of Science and ICT (22-BR-01-03) (to J.Y.M.).

Author affiliations: [a]Research Institute of Aging and Metabolism, Kyungpook National University, Daegu, 41944 Republic of Korea; [b]Leading-edge Research Center for Drug Discovery and Development for Diabetes and Metabolic Disease, Kyungpook National University, Daegu, 41404 Republic of Korea; [c]Bio-Medical Research Institute, Kyungpook National University Hospital, Daegu, 41944 Republic of Korea; [d]Department of Biomedical Science, Graduate School, Kyungpook National University, Daegu, 41944 Republic of Korea; [e]BK21 Plus KNU Biomedical Convergence Program, Kyungpook National University, Daegu, 41944 Republic of Korea; [f]Center for Genomic Integrity (CGI), Institute for Basic Science (IBS), Department of Biological Sciences, Ulsan National Institute of Science and Technology (UNIST), Ulsan, 44919 Republic of Korea; [g]Department of Internal Medicine, School of Medicine, Kyungpook National University, Kyungpook National University Chilgok Hospital, Daegu, 41404 Republic of Korea; [h]Department of Colorectal Surgery, Kyungpook National University Chilgok Hospital, School of Medicine, Kyungpook National University, Daegu, 41404 Republic of Korea; [i]Neural Circuit Research Group, Korea Brain Research Institute, Daegu, 41068 Republic of Korea; [j]Department of Biochemistry and Molecular Biology, Indiana University School of Medicine, Indianapolis, IN 46202; [k]Department of Biological Sciences, Graduate School of Science, Osaka University, Toyonaka, 560-0043 Japan; [l]Department of Protein Biochemistry, Institute of Life Science, Kurume University, Kurume, 830-0011 Japan; and [m]Department of Internal Medicine, School of Medicine, Kyungpook National University, Kyungpook National University Hospital, Daegu, 41944 Republic of Korea

1. M. Liesa, O. S. Shirihai, Mitochondrial dynamics in the regulation of nutrient utilization and energy expenditure. *Cell Metab.* **17**, 491–506 (2013).
2. S. B. Vafai, V. K. Mootha, Mitochondrial disorders as windows into an ancient organelle. *Nature* **491**, 374–383 (2012).
3. T. Wai, T. Langer, Mitochondrial dynamics and metabolic regulation. *Trends Endocrinol. Metab.* **27**, 105–117 (2016).
4. R. J. Youle, A. M. van der Bliek, Mitochondrial fission, fusion, and stress. *Science* **337**, 1062–1065 (2012).
5. J. Q. Kwong, M. S. Henning, A. A. Starkov, G. Manfredi, The mitochondrial respiratory chain is a modulator of apoptosis. *J. Cell Biol.* **179**, 1163–1177 (2007).
6. A. S. Rambold, S. Cohen, J. Lippincott-Schwartz, Fatty acid trafficking in starved cells: Regulation by lipid droplet lipolysis, autophagy, and mitochondrial fusion dynamics. *Dev. Cell* **32**, 678–692 (2015).
7. D. C. Chan, Mitochondrial fusion and fission in mammals. *Annu. Rev. Cell Dev. Biol.* **22**, 79–99 (2006).
8. B. Westermann, Mitochondrial fusion and fission in cell life and death. *Nat. Rev. Mol. Cell Biol.* **11**, 872–884 (2010).
9. S. Cogliati, J. A. Enriquez, L. Scorrano, Mitochondrial cristae: Where beauty meets functionality. *Trends Biochem. Sci.* **41**, 261–273 (2016).
10. S. Park *et al.*, Role of the pyruvate dehydrogenase complex in metabolic remodeling: Differential pyruvate dehydrogenase complex functions in metabolism. *Diabetes Metab. J.* **42**, 270–281 (2018).
11. J. H. Jeon *et al.*, Loss of metabolic flexibility as a result of overexpression of pyruvate dehydrogenase kinases in muscle, liver and the immune system: Therapeutic targets in metabolic diseases. *J. Diabetes Investig.* **12**, 21–31 (2021).
12. T. Thoudam *et al.*, PDK4 augments ER-mitochondria contact to dampen skeletal muscle insulin signaling during obesity. *Diabetes* **68**, 571–586 (2019).
13. J. R. Friedman *et al.*, ER tubules mark sites of mitochondrial division. *Science* **334**, 358–362 (2011).
14. P. Mishra, V. Carelli, G. Manfredi, D. C. Chan, Proteolytic cleavage of Opa1 stimulates mitochondrial inner membrane fusion and couples fusion to oxidative phosphorylation. *Cell Metab.* **19**, 630–641 (2014).
15. G. M. Cereghetti *et al.*, Dephosphorylation by calcineurin regulates translocation of Drp1 to mitochondria. *Proc. Natl. Acad. Sci. U.S.A.* **105**, 15803–15808 (2008).
16. O. C. Losón, Z. Song, H. Chen, D. C. Chan, Fis1, Mff, MiD49, and MiD51 mediate Drp1 recruitment in mitochondrial fission. *Mol. Biol. Cell* **24**, 659–667 (2013).
17. K. Y. Fung, L. Dai, W. S. Trimble, Cell and molecular biology of septins. *Int. Rev. Cell Mol. Biol.* **310**, 289–339 (2014).
18. A. Pagliuso *et al.*, A role for septin 2 in Drp1-mediated mitochondrial fission. *EMBO Rep.* **17**, 858–873 (2016).
19. L. D. Osellame *et al.*, Cooperative and independent roles of the Drp1 adaptors Mff, MiD49 and MiD51 in mitochondrial fission. *J. Cell Sci.* **129**, 2170–2181 (2016).
20. T. B. Fonseca, Á. Sánchez-Guerrero, I. Milosevic, N. Raimundo, Mitochondrial fission requires DRP1 but not dynamins. *Nature* **570**, E34–E42 (2019).
21. C. H. Yao *et al.*, Mitochondrial fusion supports increased oxidative phosphorylation during cell proliferation. *eLife* **8**, e41351 (2019).
22. S. Züchner *et al.*, Mutations in the mitochondrial GTPase mitofusin 2 cause Charcot-Marie-Tooth neuropathy type 2A. *Nat. Genet.* **36**, 449–451 (2004).
23. A. G. Rocha *et al.*, MFN2 agonists reverse mitochondrial defects in preclinical models of Charcot-Marie-Tooth disease type 2A. *Science* **360**, 336–341 (2018).
24. Y. Zhou *et al.*, Restoring mitofusin balance prevents axonal degeneration in a Charcot-Marie-Tooth type 2A model. *J. Clin. Invest.* **129**, 1756–1771 (2019).
25. D. Zhang *et al.*, Increased mitochondrial fission is critical for hypoxia-induced pancreatic beta cell death. *PLoS One* **13**, e0197266 (2018).
26. W. Zhang *et al.*, Hypoxic mitophagy regulates mitochondrial quality and platelet activation and determines severity of I/R heart injury. *eLife* **5**, e21407 (2016).
27. A. G. Trinidad *et al.*, Pyruvate dehydrogenase kinase 4 exhibits a novel role in the activation of mutant KRAS, regulating cell growth in lung and colorectal tumour cells. *Oncogene* **36**, 6164–6176 (2017).
28. E. R. Roberts, K. J. Thomas, The role of mitochondria in the development and progression of lung cancer. *Comput. Struct. Biotechnol. J.* **6**, e201303019 (2013).
29. P. Mishra, D. C. Chan, Mitochondrial dynamics and inheritance during cell division, development and disease. *Nat. Rev. Mol. Cell Biol.* **15**, 634–646 (2014).
30. C. J. Oh *et al.*, Pyruvate dehydrogenase kinase 4 deficiency attenuates cisplatin-induced acute kidney injury. *Kidney Int.* **91**, 880–895 (2017).
31. S. J. Lee *et al.*, Pyruvate dehydrogenase kinase 4 promotes vascular calcification via SMAD1/5/8 phosphorylation. *Sci. Rep.* **5**, 16577 (2015).
32. P. Wu *et al.*, Starvation increases the amount of pyruvate dehydrogenase kinase in several mammalian tissues. *Arch. Biochem. Biophys.* **381**, 1–7 (2000).
33. B. Y. Park *et al.*, PDK4 deficiency suppresses hepatic glucagon signaling by decreasing cAMP levels. *Diabetes* **67**, 2054–2068 (2018).
34. E. Q. Toyama *et al.*, Metabolism. AMP-activated protein kinase mediates mitochondrial fission in response to energy stress. *Science* **351**, 275–281 (2016).
35. J. A. Kashatus *et al.*, Erk2 phosphorylation of Drp1 promotes mitochondrial fission and MAPK-driven tumor growth. *Mol. Cell* **57**, 537–551 (2015).
36. H. He *et al.*, Expression of septin 2 and association with clinicopathological parameters in colorectal cancer. *Oncol. Lett.* **18**, 2376–2383 (2019).
37. M. M. Mihaylova, R. J. Shaw, The AMPK signalling pathway coordinates cell growth, autophagy and metabolism. *Nat. Cell Biol.* **13**, 1016–1023 (2011).
38. L. Hao *et al.*, ATF4 activation promotes hepatic mitochondrial dysfunction by repressing NRF1-TFAM signalling in alcoholic steatohepatitis. *Gut.* **70**, 1933–1945 (2020).
39. Y. Wang *et al.*, The role of mitochondrial dynamics and mitophagy in carcinogenesis, metastasis and therapy. *Front. Cell Dev. Biol.* **8**, 413 (2020).
40. A. Lang, A. T. John Peter, B. Kornmann, ER-mitochondria contact sites in yeast: Beyond the myths of ERMES. *Curr. Opin. Cell Biol.* **35**, 7–12 (2015).
41. M. E. Durkin, X. Qian, N. C. Popescu, D. R. Lowy, Isolation of mouse embryo fibroblasts. *Bio Protoc.* **3**, e908 (2013).
42. Y. Oligschlaeger *et al.*, The recruitment of AMP-activated protein kinase to glycogen is regulated by autophosphorylation. *J. Biol. Chem.* **290**, 11715–11728 (2015).
43. T. Thoudam, D. Chanda, Noncanonical PDK4 action alters mitochondrial dynamics to affect the cellular respiratory status, Mendeley Data, V1, doi: 10.17632/g23k3t8c83.1